Thermal and transport properties in central heavy-ion reactions around a few hundred MeV/nucleon

X. G. Deng (邓先概),[1,2] Y. G. Ma (马余刚),[1,3,*] and M. Veselský[4]
[1]*Shanghai Institute of Applied Physics, Chinese Academy of Sciences, Shanghai 201800, China*
[2]*University of Chinese Academy of Sciences, Beijing 100049, China*
[3]*ShanghaiTech University, Shanghai 200031, China*
[4]*Institute of Physics, Slovak Academy of Sciences, Dúbravská cesta 9, 84511 Bratislava, Slovakia*
(Received 18 May 2016; revised manuscript received 25 September 2016; published 28 October 2016)

The thermalization process of nuclear matter in the central fireball region of heavy-ion collisions is investigated by employing an extended Boltzmann-Uehling-Uhlenbeck model, namely, the van der Waals Boltzmann-Uehling-Uhlenbeck (VdWBUU) model. The temperature (T) is extracted by the quantum fermion fluctuation approach and other thermodynamic quantities, such as the density (ρ), entropy density (s), shear viscosity (η), isospin diffusivity (D_I), and heat conductivity (κ), are also deduced. The liquidlike and gaslike phase signs are discussed through the behavior of the shear viscosity during the heavy-ion collision process in the VdWBUU model.

DOI: 10.1103/PhysRevC.94.044622

I. INTRODUCTION

Heavy-ion collision provides a unique tool for understanding the properties of nuclear matter at different nuclear temperatures and densities and determining the nuclear equation of state (EoS) [1,2]. Many observables are required to learn the properties of the nuclear matter, such as thermodynamic variables and transport coefficients. A core observable is the nuclear temperature, which has been extensively investigated by theories and experiments using different approaches [3] like the double ratio of the isotopic yield [4,5], kinetic approaches [6–12], the isospin thermometer [13,14], the double Fermi sphere [15], the classical fluctuation method [16], and the quantum fluctuation method [17,18]. Nevertheless, there is no consensus as to the best thermometer for the nuclear system [3]. One motivation for determining the temperature is to investigate the liquid-gas phase transition in nuclear matter. In previous work [4,19–24], many authors have made efforts to study the liquid-gas phase transition in heavy-ion reactions. Classical liquid has the feature that the shear viscosity decreases with increasing temperature [25–29]. However, the situation with gas is the opposite [29,30]. For a microsystem, investigation of the shear viscosity of nuclear matter is an exciting subject.. In addition, the ratio of shear viscosity to entropy density (η/s) seems to have the bound of $\hbar/(4\pi)$, proposed by Kovtun-Son-Starinets (KSS) in certain supersymmetric gauge theory [31]. For years, attention was paid to this value of quark-gluon matter produced at relativistic energies [32–41]. However, studies on the shear viscosity of nuclear matter formed at lower energies are very limited [42–50]. In addition, in contrast with the viscosity coefficient, other transport coefficients like the heat conductivity and isospin diffusion are still less mentioned for nuclear matter. Considering the above situations, the present work focuses on studies of transport coefficients in intermediate-energy heavy-ion collisions.

The paper is organizied as follows: In Sec. II, the simulation model and calculated formalism are introduced. In Sec. III, thermal and transport results on central nuclear matter are extracted, and signals of liquidlike and gaslike phases are discussed bywith regard to the temperature-dependent shear viscosity. Finally, the conclusion is in Sec. IV.

II. THE VAN DER WAALS BOLTZMANN-UEHLING-UHLENBECK (VDWBUU) MODEL AND FORMALISM

A. van der Waals Boltzmann-Uehling-Uhlenbeck MODEL

The Boltzmann-Uehling-Uhlenbeck (BUU) model is a popular tool for describing intermediate-energy heavy-ion collisions [51,52]. As a one-body mean-field theory based on the Boltzmann equation [53], the BUU equation reads [54]

$$\frac{\partial f}{\partial t} + \upsilon\nabla_r f - \nabla_r U \nabla_p f = \frac{4}{(2\pi)^3}\int d^3p_2 d^3p_3 d\Omega \frac{d\sigma_{NN}}{d\Omega}\upsilon_{12} \times [f_3 f_4(1-f)(1-f_2) - f f_2(1-f_3)(1-f_4)]\delta^3(p+p_2-p_3-p_4), \quad (1)$$

where $f = f(r,p,t)$ is the phase-space distribution function, which can be solved using the method of Bertsch and Das Gupta [55]; $\frac{d\sigma_{NN}}{d\Omega}$ is the in-medium nucleon-nucleon cross section; and υ_{12} is the relative velocity for colliding nucleons. U is the mean-field potential including the isospin-dependent symmetry energy term,

$$U(\rho,\tau_z) = a\left(\frac{\rho}{\rho_0}\right) + b\left(\frac{\rho}{\rho_0}\right)^{\kappa} + 2a_s\left(\frac{\rho}{\rho_0}\right)^{\gamma}\tau_z I, \quad (2)$$

where $\rho_0 = 0.168$ fm^{-3} is the normal nuclear matter density; $I = (\rho_n - \rho_p)/\rho$, with ρ, ρ_n, and ρ_p being the densities of nucleons, neutrons, and protons, respectively; $\tau_z = 1$ for neutrons and $\tau_z = -1$ for protons; a_s is the coefficient of the symmetry energy term; γ describes the density dependence; and a, b, and κ are parameters for the nuclear equation of state. In this paper, we use two typical sets of mean-field parameters:

*ygma@sinap.ac.cn

the hard EoS, with a compressibility K of 380 MeV ($a = -124$ MeV, $b = 70.5$ MeV, $\kappa = 2$); and the soft EoS, with a K of 200 MeV ($a = -356$ MeV, $b = 303$ MeV, $\kappa = 7/6$). In the model, the Coulomb interaction is also considered.

There are different versions of the BUU model. The main differences are the extension of improvement potential and degree of freedom of isospin, which is explicitly taken into account [56]. Here we use the version of the VdWBUU model which was developed by Veselský and Ma [57]. The pressure (p) changes in the thermodynamical EoS, as a measure of nonideality of a neutron or a proton gas, can be defined as

$$p = \rho^2 \frac{\partial \mathcal{U}}{\partial \rho}, \tag{3}$$

where $\mathcal{U}$ is the thermodynamic potential. When $\mathcal{U}$ is evaluated as the sum of the single-particle contributions of neutrons and protons, shown in Eq. (2), Eq. (4) can be obtained,

$$p = \left(\frac{f_{5/2}(z)}{f_{3/2}(z)}\right)\rho T + a\rho^2 + b\kappa\rho^{1+\kappa} + 2\gamma a_s \rho_0 \left(\frac{\rho}{\rho_0}\right)^{1+\gamma} \tau_z I, \tag{4}$$

where $z = \exp(\mu/T)$ is the fugacity value of nucleons, with μ being the chemical potential and T the temperature; and $\frac{f_{5/2}(z)}{f_{3/2}(z)}$ is a factor, a fraction of the Fermi integrals $f_n(z) = \frac{1}{\Gamma(n)} \int_0^\infty \frac{x^{n-1}}{z^{-1}e^x+1} dx$. Based on the van der Waals EoS, using the particle density ρ, one can obtain

$$(p + a'\rho^2)(1 - \rho b') = \left(\frac{f_{5/2}(z)}{f_{3/2}(z)}\right)\rho T, \tag{5}$$

where a' is related to the attractive interaction among particles and b' denotes the proper volume of the constituent particle, which can be related geometrically to its cross section for interaction with other particles. Comparing Eq. (4) with Eq. (5), one has

$$a' = -a, \tag{6}$$

$$b' = \frac{b\kappa\rho^\kappa + 2\gamma a_s \left(\frac{\rho}{\rho_0}\right)^{1+\gamma} \tau_z I}{\left(\frac{f_{5/2}(z)}{f_{3/2}(z)}\right)\rho T + b\kappa\rho^{1+\kappa} + 2\gamma a_s \rho_0 \left(\frac{\rho}{\rho_0}\right)^{1+\gamma} \tau_z I}. \tag{7}$$

In a system composed of nucleons, the proper volume can be used to estimate its cross section within the nucleonic medium,

$$\sigma = \left(\frac{9\pi}{16}\right)^{1/3} b'^{2/3}, \tag{8}$$

which can be implemented into the collision term of the BUU equation. In this way, the BUU can be simulated with both isospin-dependent mean-field and nucleon-nucleon cross sections, which are correlated with each other. This is the so-called VdWBUU equation. More details can be found in Ref. [57].

B. Evaluated formalism

In this paper, the thermodynamic and transport properties of a nuclear system are investigated in the framework of the VdWBUU approach. Thermodynamic quantities are extracted with different formalisms.

The concept of nuclear temperature was proposed by Bethe [58] and Weisskopf [59]. Different thermometer methods to extract the nuclear temperature are given in Ref. [3]. In Refs. [15] and [46], the hot Thomas-Fermi formalism was used to calculate the temperature. In this paper, a method based on quantum fluctuation of fermions is applied to calculate the temperature, proposed in Ref. [17]. The quadrupole $Q_{xy} = p_x^2 - p_y^2$ is defined and the variance $\langle\sigma_{xy}^2\rangle$ is given in Ref. [16],

$$\langle\sigma_{xy}^2\rangle = \int d^3p \left(p_x^2 - p_y^2\right)^2 n(p), \tag{9}$$

where $n(p)$ is the momentum distribution of particles. In heavy-ion collisions, protons, neutrons, and tritium follow Fermi statistics, thus the Fermi-Dirac distribution can be used in Eq. (9) [16]. Using the Fermi-Dirac distribution $n(p)$, we have

$$\begin{aligned}\langle\sigma_{xy}^2\rangle &= \frac{\int d^3p \left(p_x^2 - p_y^2\right)^2 n(p)}{\int d^3p\, n(p)} \\ &= (2mT)^2 \frac{4}{15} \frac{\int_0^\infty y^{\frac{5}{2}} \frac{1}{z^{-1}e^y+1} dy}{\int_0^\infty y^{\frac{1}{2}} \frac{1}{z^{-1}e^y+1} dy} \\ &= (2mT)^2 F_{QC}(z),\end{aligned} \tag{10}$$

where $z = \exp(\mu/T)$, and $F_{QC}(z)$ is the quantum correction factor. The chemical potential (μ) can be extracted using the following equation [47]:

$$\begin{aligned}\rho_\tau &= \frac{g}{(2\pi\hbar)^3} \int n_\tau(p) d^3p \\ &= \frac{1}{2\pi^2} \left(\frac{2m}{\hbar^2}\right)^{\frac{3}{2}} \int_0^\infty \frac{\sqrt{y}}{z_\tau^{-1}e^y + 1} dy.\end{aligned} \tag{11}$$

Here g (=2) is the spin degeneracy of the nucleon and τ denotes n for neutron or p for proton. With the variance $\langle\sigma_{xy}^2\rangle$, chemical potential, and density calculated using data from the spatial distribution of test particles, the temperature of the nuclear system can be extracted. The entropy density can be obtained by a given density and temperature [60],

$$s = \frac{U - A}{T} \frac{1}{V} = \left[\frac{5}{2} \frac{f_{5/2}(z)}{f_{3/2}(z)} - \ln z\right]\rho, \tag{12}$$

where U is the internal energy and A is the Helmholtz free energy [61].

In order to learn more about the properties of hot nuclei during heavy-ion collisions or the nuclear EoS, the transport coefficients are evaluated, including the shear viscosity (η), isospin diffusivity (D_I), and heat conductivity (κ). In hydrodynamics, internal friction occurs when relative motions exist in a fluid (liquid or gas), and this is called viscosity. The shear viscosity depends on many factors of the fluid species: the velocity gradient, temperature, and density. The diffusivity is a measure of the rate at which particles or heat or fluids can spread. Here, the isospin diffusivity represents the capability of isospin diffusion in nuclear matter. The heat conductivity represents the ability of a material to conduct heat. These three transport coefficients are important for the nucleonic transport process of nuclear matter and were discussed in

Ref. [62] for a two-component nuclear Fermi system. By solving the Boltzmann-equation set such as used in reaction simulations [55], the numerical results for the coefficients have been obtained,

$$\eta(\rho,T,I) = (1+0.10I^2)\left[\frac{856}{T^{1.10}}\left(\frac{\rho}{\rho_0}\right)^{1.81} - \frac{240.9}{T^{0.95}}\left(\frac{\rho}{\rho_0}\right)^{2.12} + 2.154T^{0.75}\right], \quad (13)$$

$$D_I(\rho,T,I) = (1-0.19I^2)\left[\frac{11.34}{T^{2.38}}\left(\frac{\rho}{\rho_0}\right)^{1.54} + \frac{1.746}{T}\left(\frac{\rho}{\rho_0}\right)^{0.56} + 0.00585T^{0.913}\left(\frac{\rho}{\rho_0}\right)\right], \quad (14)$$

$$\kappa(\rho,T,I) = (1+0.10I^2)\left[\frac{0.235}{T^{0.755}}\left(\frac{\rho}{\rho_0}\right)^{0.951} - 0.0582\left(\frac{\rho}{\rho_0}\right)^{0.0816} + 0.0238T^{0.5627}\left(\frac{\rho}{\rho_0}\right)^{0.0171}\right], \quad (15)$$

where T is the temperature in MeV, η is the shear viscosity in MeV/(fm$^2\,c$), D_I is the isospin diffusivity in fm $\cdot\, c$, the heat conductivity κ is in c/fm^2; and $I = \frac{\rho_n-\rho_p}{\rho}$ is the isospin asymmetry. More details can be found in Ref. [62]. The numerical results for these coefficients are calculated by using the experimentally measured nucleon-nucleon cross section $\sigma_{\rm free} = 40$ mb. More accurately, we have to modify these transport coefficients by the in-medium N-N cross sections (σ) that we adopted in Ref. [46], which can be extracted with Eqs. (7) and (8):

$$\eta(\rho,T,I,\sigma) = \frac{\eta(\rho,T,I)}{\sigma/\sigma_{\rm free}}, \quad (16)$$

$$D_I(\rho,T,I,\sigma) = \frac{D_I(\rho,T,I)}{\sigma/\sigma_{\rm free}}, \quad (17)$$

$$\kappa(\rho,T,I,\sigma) = \frac{\kappa(\rho,T,I)}{\sigma/\sigma_{\rm free}}. \quad (18)$$

III. RESULTS AND DISCUSSION

Central collisions ($b = 0$ fm) of ^{197}Au + ^{197}Au are simulated at beam energies of 100–300 MeV/nucleon, employing the VdWBUU model with the hard EoS and soft EoS. The central region is defined as a $[-5,5]^3$ fm^3 or $[-3,3]^3$ fm^3 box with its center located in the c.m. We denote that $t = 0$ fm/c is at the point where two nuclei touch initially.

A. Properties of thermodynamic quantities

Figure 1 shows the time evolution of the average density in the central region, $[-5,5]^3$ fm^3 or $[-3,3]^3$ fm^3, at incident energies of 100–300 MeV/nucleon with the hard or soft EoS. One sees that the average density is 1.2–1.6 times the normal nuclear matter density, with larger maxima at earlier times with higher beam energies. At the expansion stage, higher beam energies lead rapidly to lower densities. At the same incident energy, comparing Fig. 1(a) with Fig. 1(c), the densities of the hard EoS and soft EoS are similar; however, comparing Fig. 1(a) with Fig. 1(b), or Fig. 1(c) with Fig. 1(d), the density is higher in the smaller region at the maximum point. The reason is that the density of the zone far from the center is lower than that of the close one.

The time evolution of the average temperature is shown in Fig. 2. At the initial stage the average temperature is nearly 0 because the two nuclei are cold with Fermi momenta at the beginning of the collision. As the two nuclei come close to each other, with increasing nucleon-nucleon collisions, the temperature increases and reaches a maximum of 13–48 MeV, and it is higher at higher incident energies. At the expansion stage, the temperature decreases and falls more rapidly at higher incident energies. Comparing Fig. 2(a) with Fig. 2(c), the maximum temperature with the hard EoS is lower than that with the soft EoS. This indicates that the collision with the soft EoS is compressed more easily than that with the hard one and more beam motions are transformed into thermal motions. Along the time scale of the collision, the maximumtemperature points at different beam energies in Fig. 2(a) or Fig. 2(c) are delayed in comparison with the maximum density points in Fig. 1(a) or Fig. 1(c), indicating that nucleon-nucleon collisions are still frequent when the maximum compression is reached. The features in Fig. 2(c) are similar to those reported by Zhou *et al.* [46], who used the Thomas-Fermi method to

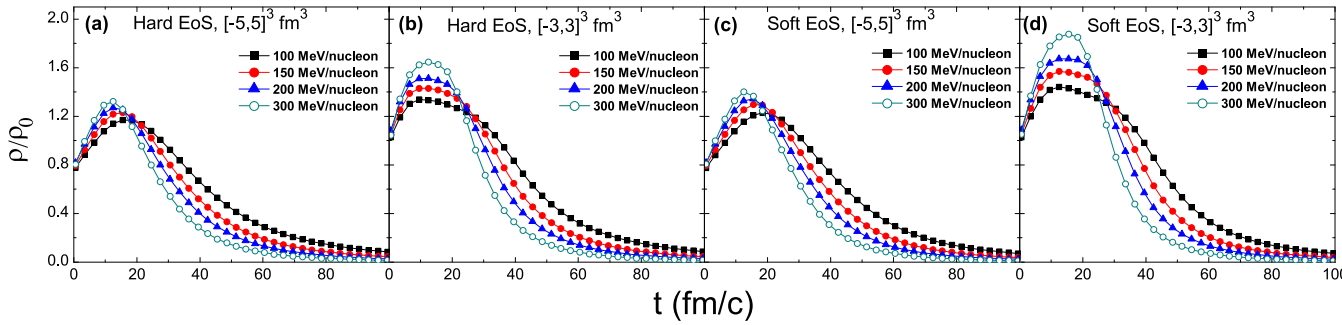

FIG. 1. Time evolution of the average density at different incident energies for (a) the hard EoS in the region of $X[-5,5]$, $Y[-5,5]$, $Z[-5,5]$; (b) the hard EoS in the region of $X[-3,3]$, $Y[-3,3]$, $Z[-3,3]$; (c) the soft EoS in the region of $X[-5,5]$, $Y[-5,5]$, $Z[-5,5]$; and (d) the soft EoS in the region of $X[-3,3]$, $Y[-3,3]$, $Z[-3,3]$.

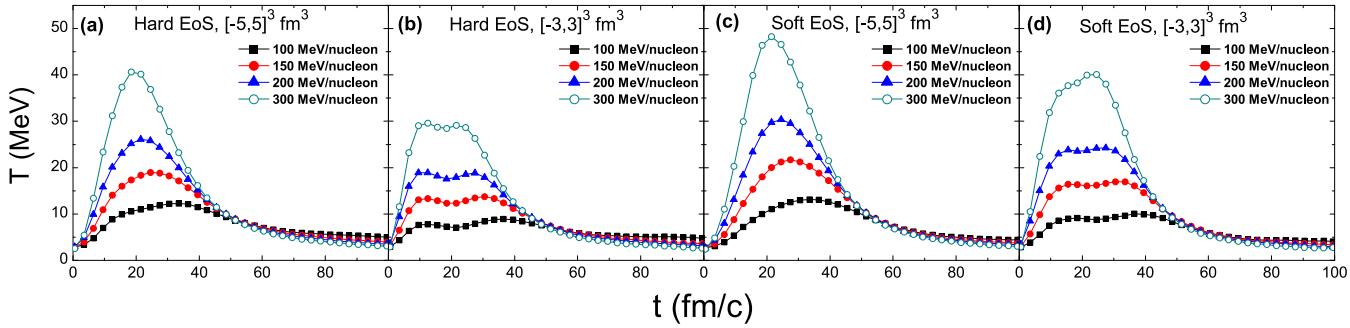

FIG. 2. Time evolution of the average temperature at different incident energies. The conditions are the same as in Fig. 1.

obtain the temperature with the isospin-dependent quantum molecular dynamics (IQMD) model for a central spherical region with a radius of 5 fm. Of course, the quantitative value of the temperature depends on the model and thermometer. Meanwhile, in Figs. 2(b) and 2(d) in the $[-3,3]^3$ fm^3 region, the average temperature remains saturated near the peak point. The size effect is obvious. A smaller central region has fewer nucleons, thus more interaction information may not be included. So if one wants to extract the information from the central region, a suitable size should be considered. To simplify the structure of the present paper, we present the following calculation results just with the soft EoS. Of course, the case with the hard EoS maintains similar qualitative behaviors.

Time evolutions of the average entropy density and entropy per nucleon are shown in Fig. 3. Since the system is an open system with nonfixed nucleon numbers, the information on the entropy per nucleon will be interesting. During the compression process between two nuclei, the nucleon number in the region and state numbers of the system will increase natrally, hence the increase in average entropy density. Conversely, it decreases at the expansion stage. The time evolution of the average entropy density is similar to the case for the average temperature, i.e., a higher beam energy leads to a higher entropy density at the maximum value of 0.1–0.7 fm^{-3}. This shows that the higher the beam energy and the higher the internal energy in the central region, the greater the state numbers and entropy will be. However, at different incident energies, the average entropy densities reach the maximum earlier than the average temperatures (discussed later). At the expansion stage, the average entropy density decreases. And the entropy per nucleon more or less shows saturation at a higher beam energy, but it shows a slight increase with time at a lower one, indicating the potential of the open system to convert slowly to internal energy after maximum compression for the lower incident energy. In other words, the central fireball tends to equilibration more rapidly at a higher incident energy.

The shear viscosity, isospin diffusivity, and heat conductivity are shown in Fig. 4. The shear viscosity, isospin diffusivity, and heat conductivity decrease drastically in the initial compression stage (0–20 fm/c). The shear viscosity and isospin diffusivity tend to an asymptotic value after 20 fm/c, respectively, while the heat conductivity shows a peak around 20 fm/c, indicating that the compressed nuclear matter has a greater heat conduction capability at the stage of higher temperature and higher density.

In Fig. 5, the ratio of shear viscosity to entropy density also decreases drastically in the initial compression stage (0–20 fm/c) and tends to an asymptotic value after 20 fm/c. It is noted that the lower value of the ratio of shear viscosity to entropy density is found at a higher incident energy during early time evolution. Overall, η/s values approximate asymptotic values above the KSS bound of $\sim\frac{\hbar}{4\pi}$ at the expansion stage.

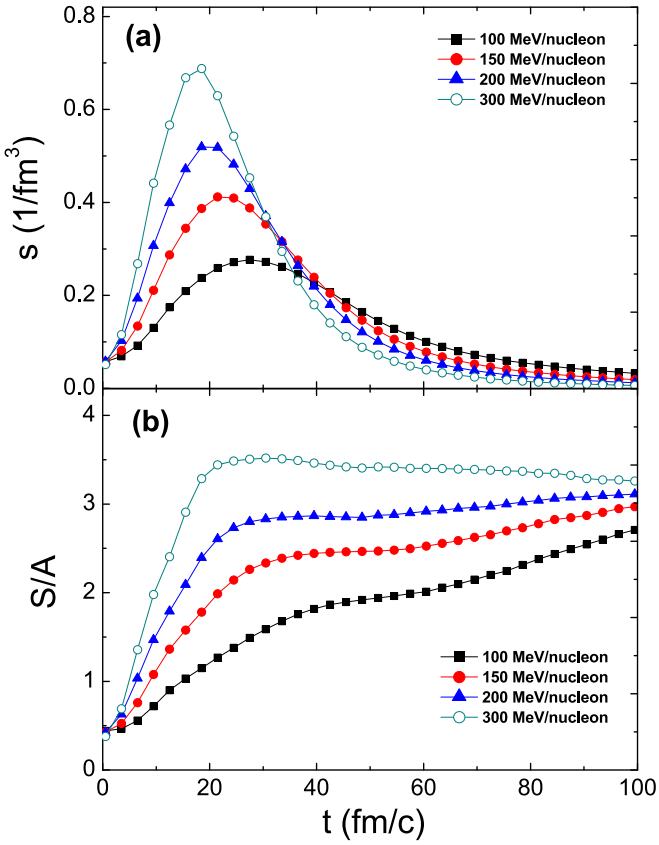

FIG. 3. Time evolution of the average entropy density (a) and entropy per nucleon (b) at different incident energies for the soft EoS in the region of $X[-5,5]$, $Y[-5,5]$, and $Z[-5,5]$.

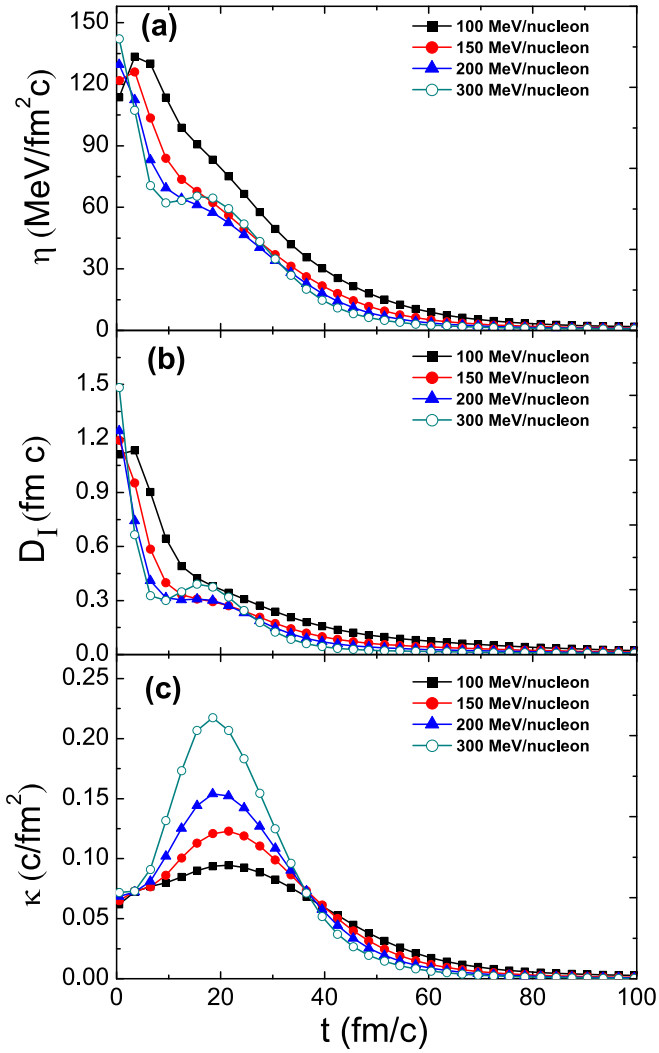

FIG. 4. Time evolution of the shear viscosity (a), isospin diffusivity (b), and heat conductivity (c) at different incident energies for the soft EoS in the region of $X[-5,5]$, $Y[-5,5]$, and $Z[-5,5]$.

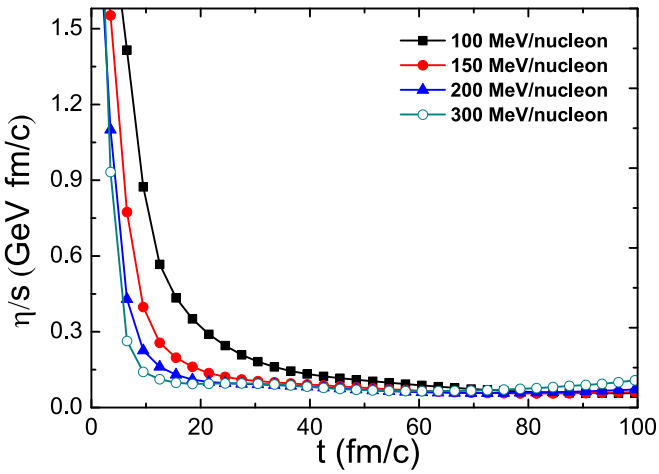

FIG. 5. Time evolution of the ratio of shear viscosity to entropy density at different incident energies for the soft EoS in the region of $X[-5,5]$, $Y[-5,5]$, and $Z[-5,5]$.

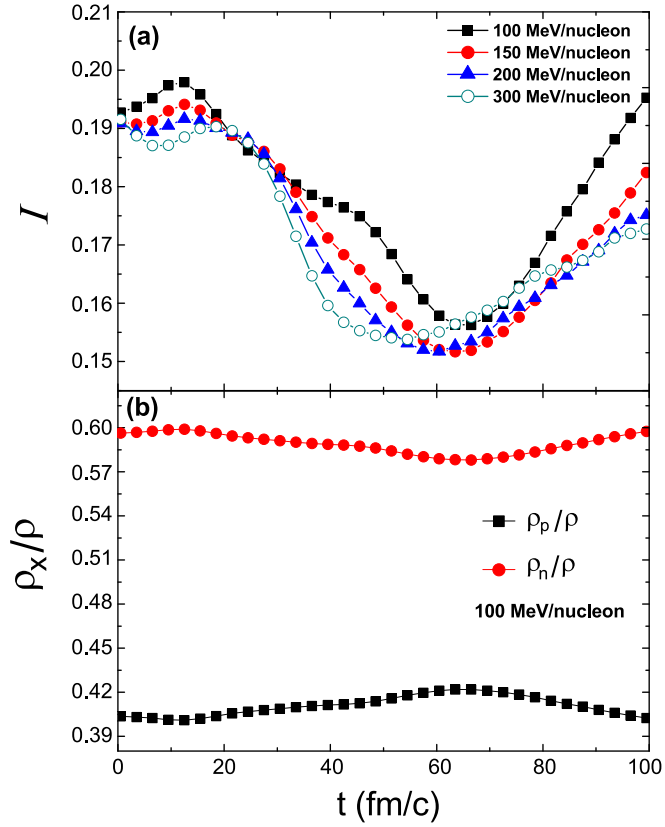

FIG. 6. Time evolution of the isospin asymmetry at different incident energies (a) and various reduced densities (ρ_n, ρ_p, and ρ represent the neutron, proton, and total densities, respectively; x is n or p) at 100 MeV/nucleon (b) for the soft EoS in the region of $X[-5,5]$, $Y[-5,5]$, and $Z[-5,5]$.

In Fig. 6(a), the isospin asymmetry (I) changes little before 20 fm/c but drops to a minimum at ∼60 fm/c and then increases again. At lower energies, the valley of I is a relative shallow. This valley is associated with the density evolutions of neutrons and protons. For instance, the evolutions of reduced density of neutrons and protons over the total density at an incident energy of 100 MeV/nucleon are shown in Fig. 6(b). Obviously, the reduced density of neutrons generally decreases before ∼60 fm/c and vice versa for the reduced density of protons. Therefore, the isospin, defined as $(\rho_n - \rho_p)/\rho$, shows a dip around 60 fm/c in Fig. 6(a). This dip point induces an inflection point of isospin diffusivity versus isospin asymmetry as shown in Fig. 7.

In the above figures, peaks or valleys of some quantities observed during their time evolution are more or less related to the transformation from the compression stage to the expansion stage in heavy-ion collisions. To compare the corresponding times at which the peaks or valleys for various observables, such as density, temperature, entropy density, and isospin asymmetry, reach a maximum or minimum, we can compare different time orders of these quantities. Figure 8 shows the corresponding times at the peak or valley of these quantities as a function of the beam energy. One can roughly see that every above quantity decreases with increasing incident energy.

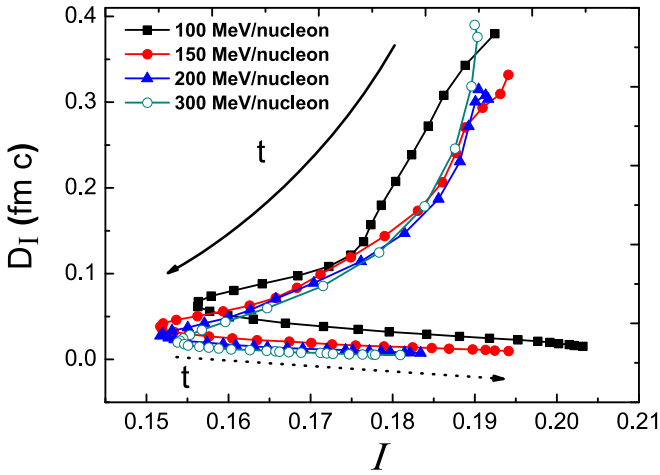

FIG. 7. Isospin diffusivity as a function of the isospin asymmetry at $t = 15$–100 fm/c at different incident energies for the soft EoS in the region of $X[-5,5]$, $Y[-5,5]$, and $Z[-5,5]$. Solid and dotted arrows indicate the early and later processes of expansion, respectively.

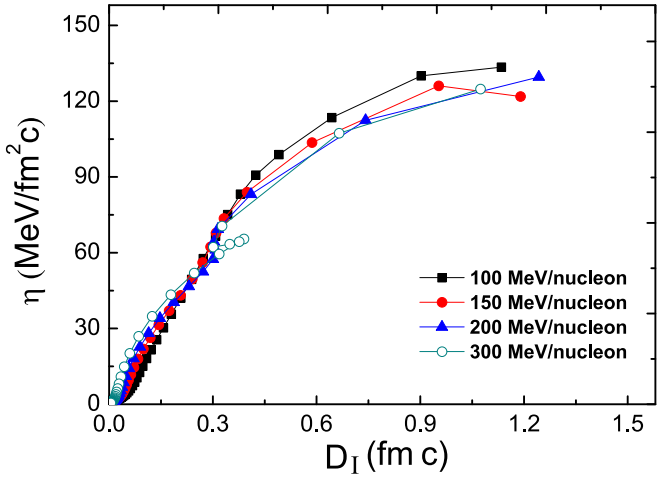

FIG. 9. Shear viscosity as a function of isospin diffusivity at different incident energies for the soft EoS in the region of $X[-5,5]$, $Y[-5,5]$, $Z[-5,5]$.

Note that the time point at which the temperature reaches its maximum at different incident energies is later than that at which the maximum density is reached. This indicates that even when the maximum compressed state is reached, frequent nucleon-nucleon collisions are still occurring and therefore the system is still heating. The time points at which the entropy density reaches its maximum are between those of the maximum density and maximum temperature. This indicates that when the system reaches the maximum compression stage in the central region, the internal energy increases with the NN collision leading to increasing numbers of states and therefore the entropy density is still increasing at that time. In contrast, the isospin asymmetry reaches its minimum much later in comparison with other observables since it is mostly due to the isospin transport process and not directly related to the compression-expansion process.

As shown in Fig. 9, the isospin diffusivity shows a monotonic dependence on the shear viscosity, indicating that the viscous nuclear matter favors isospin diffusion. In Fig. 10, the heat conductivity increases as the temperature at the compression stage, which is similar to classical behavior [62]. Finally, heat conductivity drops at the expansion stage. During the compression stage, more frequent NN collisions lead to a hotter and higher heat conductivity of the system. At the expansion stage, however, the system cools down with a lower heat conductivity.

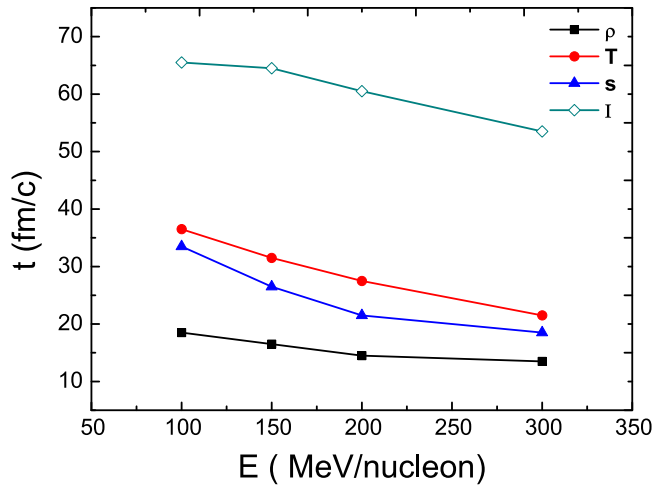

FIG. 8. Time points of the maximum average density (filled squares), maximum average entropy density (open triangles), maximum average temperature (filled circles), and minimum isospin asymmetry (open diamonds) as a function of the beam energy for the soft EoS in the region of $X[-5,5]$, $Y[-5,5]$, and $Z[-5,5]$.

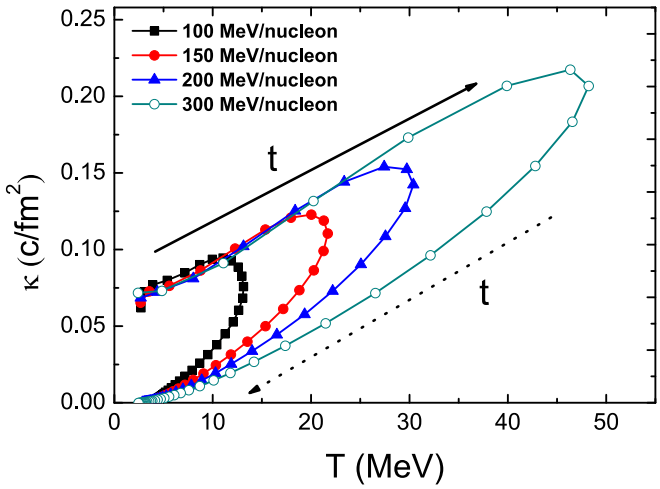

FIG. 10. Heat conductivity as a function of temperature at different incident energies for the soft EoS in the region of $X[-5,5]$, $Y[-5,5]$, and $Z[-5,5]$. Filled and dotted arrows indicate the compression process and expansion process, respectively.

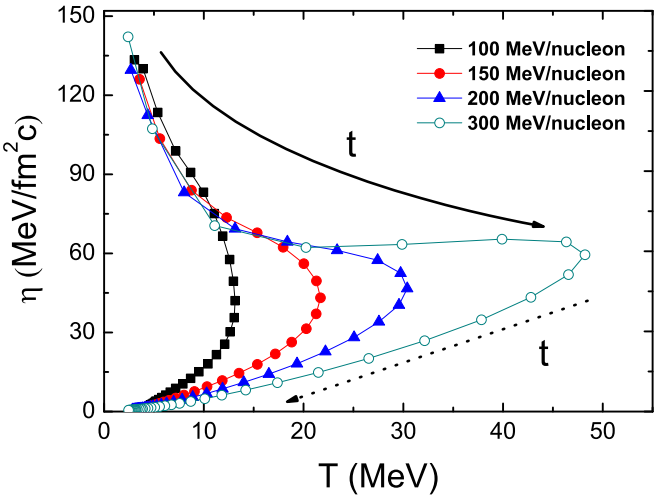

FIG. 11. Shear viscosity as a function of temperature at different incident energies for the soft EoS in the region of $X[-5,5]$, $Y[-5,5]$, and $Z[-5,5]$. Filled and dotted arrows indicate the compression process and expansion process, respectively.

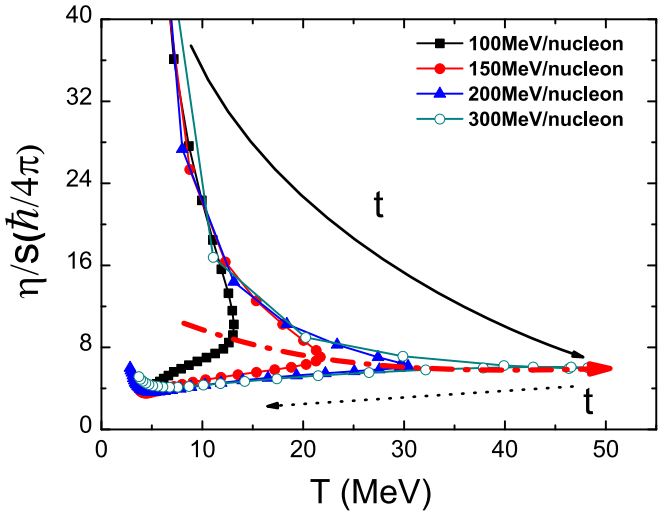

FIG. 12. Ratio of the shear viscosity to the entropy density, in units of $\frac{\hbar}{4\pi}$, as a function of the temperature at different incident energies for the soft EoS in the region of $X[-5,5]$, $Y[-5,5]$, and $Z[-5,5]$. The dashed red line shows the trend of the η/s value at the turning point with the temperature.

B. The signature of liquidlike and gaslike phases

The relationship between shear viscosity and temperature differs in liquid and gas of common substances. In the present study on a matter system, we find similar behaviors of liquidlike and gaslike phases in the quantities we extracted. It should be mentioned that, in Fig. 11, the branch above the inflection point at different beam energies represents the compression process, and the bottom branch the expansion process. One finds that in the compression process, the shear viscosity decreases with increasing temperature, while in the expansion process the behavior is inverse. We also note that in classical liquid, as the temperature gets higher, a decrease in shear viscosity [26] also occurs. On the contrary, the shear viscosity of gas [30] and meson gas [63] drops with a decrease in temperature as the collision probability becomes lower. More information can be obtained from Refs. [25,27,28,64,65]. In this context, it is analogous that nuclear matter is in the liquidlike phase during the compression process, while it is in the gaslike phase during the later expansion process. Around the inflection point the system is in a kind of mixedlike phase.

C. η/s versus temperature or beam energy

As shown in Fig. 5, η/s reaches an asymptotic value which is above the KSS bound at the later stage when the system is fully expanded. Figure 12 shows the ratio of shear viscosity to entropy density as a function of the temperature. It is noted that when the system reaches the maximum temperature, there exists a turning point of η/s. This behavior is qualitatively consistent with the feature of η as a function of the temperature (Fig. 11). Furthermore, if we observe the behavior of η/s values at the point of maximum temperature (dashed red line in the figure), it shows that these ratios show a fast drop at a higher beam energy and reach a plateau about six times the KSS bound as other models show [45].

IV. CONCLUSIONS

In summary, thermal and transport quantities for nuclear matter formed in central Au + Au collisions at a few hundred MeV/nucleon are obtained from the VdWBUU model. The properties of the central region of the nuclear reaction are discussed with some quantities for different fireball sizes and nuclear equations of state. Time evolutions of the density, temperature, entropy density, isospin diffusivity, shear viscosity, heat conductivity, etc., are presented, which provide information on the nuclear matter of the collision system. The peak or valley behavior in the time evolution of the density, temperature, entropy, and isospin is more or less related to the compression and expansion process in heavy-ion collisions, with different time delays for the above different observables after the most compressed state. The time order of the quantities has been reported. The sign of liquidlike and gaslike phases is given by relations of the shear viscosity as a function of the temperature. The values of η/s at the maximum temperature for different beam energies demonstrate decreasing behavior and tends to an asymptotic value of $\sim 6\frac{\hbar}{4\pi}$.

ACKNOWLEDGMENTS

This work was supported in part by the National Natural Science Foundation of China under Contract Nos. 11421505 and 11220101005 and by the Major State Basic Research Development Program in China under Contract No. 2014CB845401. M.V. is grateful for the support of Chinese Academy of CAS President's International Fellowship Initiative No. 2011T2J13, the Slovak Research and Development Agency under Contract No. APVV-15-0225 and the Slovak Scientific Grant Agency under Contract No. 2/0121/14.

[1] B. A. Li, L. W. Chen, and C. M. Ko, Phys. Rep. **464**, 113 (2008).
[2] G. Giuliani, H. Zheng, and A. Bonasera, Prog. Part. Nucl. Phys. **76**, 116 (2014).
[3] A. Kelić, J. B. Natowitz, and K. H. Schmidt, Eur. Phys. J. A **30**, 203 (2006).
[4] J. Pochodzalla *et al.*, Phys. Rev. Lett. **75**, 1040 (1995).
[5] J. Wang *et al.*, Phys. Rev. C **72**, 024603 (2005).
[6] G. D. Westfall, Phys. Lett. B **116**, 118 (1982).
[7] B. V. Jacak *et al.*, Phys. Rev. Lett. **51**, 1846 (1983).
[8] G. D. Westfall, R. G. Sextro, A. M. Poskanzer, A. M. Zebelman, G. W. Butler, and E. K. Hyde, Phys. Rev. C **17**, 1368 (1978).
[9] T. Odeh *et al.*, Phys. Rev. Lett. **84**, 4557 (2000).
[10] J. Gosset, H. H. Gutbrod, W. G. Meyer, A. M. Poskanzer, A. Sandoval, R. Stock, and G. D. Westfall, Phys. Rev. C **16**, 629 (1977).
[11] D. G. d'Enterria *et al.*, Phys. Lett. B **538**, 27 (2002).
[12] R. Ortega *et al.*, Nucl. Phys. A **734**, 542 (2004).
[13] K.-H. Schmidt *et al.*, Phys. Lett. B **300**, 313 (1993).
[14] K.-H. Schmidt *et al.*, Nucl. Phys. A **710**, 157 (2002).
[15] D. T. Khoa *et al.*, Nucl. Phys. A **542**, 671 (1992).
[16] S. Wuenschel *et al.*, Nucl. Phys. A **843**, 1 (2010).
[17] H. Zheng and A. Bonasera, Phys. Lett. B **696**, 178 (2011).
[18] H. Zheng, G. Giuliani, and A. Bonasera, Nucl. Sci. Tech. **24**, 050512 (2013).
[19] Y. G. Ma *et al.*, Phys. Lett. B **390**, 41 (1997).
[20] J. Schnack and H. Feldmeier, Phys. Lett. B **409**, 6 (1997).
[21] B. K. Sharma and S. Pal, Phys. Rev. C **81**, 064304 (2010).
[22] Y. G. Ma, Phys. Rev. Lett. **83**, 3617 (1999).
[23] Y. G. Ma *et al.*, Phys. Rev. C **71**, 054606 (2005).
[24] J. B. Natowitz, K. Hagel, Y. Ma, M. Murray, L. Qin, R. Wada, and J. Wang, Phys. Rev. Lett. **89**, 212701 (2002).
[25] E. N. da, C. Andrade, Philos. Mag. **17**, 497 (1934).
[26] T. W. Chapman, Am. Inst. Chem. Eng. J. **12**, 395 (1966).
[27] J. Kestin, M. Sokolov, and W. A. Wakeham, J. Phys. Chem. Ref. Data **7**, 941 (1978).
[28] L. Battezzati and A. L. Greer, Acta Metall. **37**, 1791 (1989).
[29] M. Batzle and Z. J. Wang, Geophysics **57**, 1396 (1992).
[30] C. Beal, Soc. Petr. Eng. AIME **165**, 95 (1946).
[31] P. K. Kovtun, D. T. Son, and A. O. Starinets, Phys. Rev. Lett. **94**, 111601 (2005).
[32] A. Nakamura and S. Sakai, Phys. Rev. Lett. **94**, 072305 (2005).
[33] S. Gavin and M. Abdel-Aziz, Phys. Rev. Lett. **97**, 162302 (2006).
[34] R. Lacey *et al.*, Phys. Rev. Lett. **98**, 092301 (2007).
[35] A. Majumder, B. Müller, and X. N. Wang, Phys. Rev. Lett. **99**, 192301 (2007).
[36] Z. Xu and C. Greiner, Phys. Rev. Lett. **100**, 172301 (2008).
[37] N. Demir and S. A. Bass, Phys. Rev. Lett. **102**, 172302 (2009).
[38] J. Noronha-Hostler, J. Noronha, and C. Greiner, Phys. Rev. Lett. **103**, 172302 (2009).
[39] M. Luzum and P. Romatschke, Phys. Rev. Lett. **103**, 262302 (2009).
[40] I. Bouras *et al.*, Phys. Rev. Lett. **103**, 032301 (2009).
[41] H. Song, S. A. Bass, U. Heinz, T. Hirano, and C. Shen, Phys. Rev. Lett. **106**, 192301 (2011).
[42] N. Auerbach and S. Shlomo, Phys. Rev. Lett. **103**, 172501 (2009).
[43] D. D. Nguyen, Phys. Rev. C **84**, 034309 (2011).
[44] S. X. Li, D. Q. Fang, Y. G. Ma, and C. L. Zhou, Phys. Rev. C **84**, 024607 (2011); Nucl. Sci. Tech. **22**, 235 (2011).
[45] C. L. Zhou, Y. G. Ma, D. Q. Fang, S. X. Li, and G. Q. Zhang, Europhys. Lett. **98**, 66003 (2012).
[46] C. L. Zhou, Y. G. Ma, D. Q. Fang, and G. Q. Zhang, Phys. Rev. C **88**, 024604 (2013).
[47] D. Q. Fang, Y. G. Ma, and C. L. Zhou, Phys. Rev. C **89**, 047601 (2014).
[48] C. L. Zhou, Y. G. Ma, D. Q. Fang, G. Q. Zhang, J. Xu, X. G. Cao, and W. Q. Shen, Phys. Rev. C **90**, 057601 (2014); C. L. Zhou, Y. G. Ma, D. Q. Fang *et al.*, Nucl. Tech. **37**, 100516 (2014) [in Chinese].
[49] J. Xu, L. W. Chen, C. M. Ko, B. A. Li, and Y. G. Ma, Phys. Lett. B **727**, 244 (2013); J. Xu, Nucl. Sci. Tech. **22**, 050514 (2013).
[50] S. Pal, Phys. Rev. C **81**, 051601(R) (2010).
[51] G. F. Bertsch, H. Kruse, and S. Das Gupta, Phys. Rev. C **29**, 673 (1984).
[52] H. Kruse, B. V. Jacak, and H. Stöcker, Phys. Rev. Lett. **54**, 289 (1985).
[53] C. Y. Wong and H. H. K. Tang, Phys. Rev. Lett. **40**, 1070 (1978).
[54] W. Bauer, G. F. Bertsch, W. Cassing, and U. Mosel, Phys. Rev. C **34**, 2127 (1986).
[55] G. F. Bertsch and S. Das Gupta, Phys. Rep. **160**, 189 (1988).
[56] B. A. Li, C. M. Ko, and Z. Z. Ren, Phys. Rev. Lett. **78**, 1644 (1997).
[57] M. Veselský and Y. G. Ma, Phys. Rev. C **87**, 034615 (2013).
[58] H. A. Bethe, Rev. Mod. Phys. **9**, 69 (1937).
[59] V. F. Weisskopf, Phys. Rev. **52**, 295 (1937).
[60] H. Zheng and A. Bonasera, Phys. Rev. C **86**, 027602 (2012).
[61] L. Landau and F. Lifshits, *Statistical Physics* (Pergamon, New York, 1980); K. Huang, *Statistical Mechanics*, 2nd ed. (Wiley, New York, 1987); R. K. Pathria, *Statistical Mechanics*, 2nd ed. (Elsevier, New York, 2003).
[62] L. Shi and P. Danielewicz, Phys. Rev. C **68**, 064604 (2003).
[63] A. Muronga, Phys. Rev. C **69**, 044901 (2004).
[64] L. D. Eicher and B. J. Zwolinski, J. Phys. Chem. **75**, 2016 (1971).
[65] Y. L. Sun, M. H. Sun, W. D. Cheng, C. X. Ma, and F. Liu, Comput. Mater. Sci. **38**, 737 (2007).